Biogeosciences Discuss., 12, 12851–12897, 2015
www.biogeosciences-discuss.net/12/12851/2015/
doi:10.5194/bgd-12-12851-2015

Biogeosciences Discussions
Open Access

Climate change impacts on net primary production (NPP) and export production (EP) regulated by increasing stratification and phytoplankton community structure in CMIP5 models

W. Fu, J. Randerson, and J. K. Moore

Department of Earth System Science, University of California, Irvine, California, 92697, USA

Received: 16 June 2015 – Accepted: 17 July 2015 – Published: 12 August 2015

Correspondence to: W. Fu (weiweif@uci.edu)

Published by Copernicus Publications on behalf of the European Geosciences Union.

Abstract

We examine climate change impacts on net primary production (NPP) and export production (sinking particulate flux; EP) with simulations from nine Earth System Models (ESMs) performed in the framework of the fifth Coupled Model Inter-comparison Project (CMIP5). Global NPP and EP are reduced considerably by the end of the century for the intense warming scenario of Representative Concentration Pathway (RCP) 8.5. Relative to the 1990s, global NPP in the 2090s is reduced by 2.3–16 % and EP by 7–18 %. The models with the largest increases in stratification (and largest relative reductions in NPP and EP) also show the largest positive biases in stratification for the contemporary period, suggesting some potential overestimation of climate impacts on NPP and EP. All of the CMIP5 models show an increase in stratification in response to surface ocean warming and freshening that is accompanied by decreases in NPP, EP, and surface macronutrient concentrations. There is considerable variability across models in the absolute magnitude of these fluxes, surface nutrient concentrations, and their perturbations by climate change, indicating large model uncertainties. The negative response of NPP and EP to stratification increases reflects a bottom-up control, as nutrient flux to the euphotic zone declines. Models with dynamic phytoplankton community structure show larger declines in EP than in NPP. This is driven by phytoplankton community composition shifts, with a reduced percentage of NPP by large phytoplankton under RCP 8.5, as smaller phytoplankton are favored under the increasing nutrient stress. Thus, projections of the NPP response to climate change in the CMIP5 models are critically dependent on the simulated phytoplankton community structure, the efficiency of the biological pump, and the resulting (highly variable) levels of regenerated production. Community composition is represented relatively simply in the CMIP5 models, and should be expanded to better capture the spatial patterns and the changes in export efficiency that are necessary for predicting climate impacts on NPP.

BGD

12, 12851–12897, 2015

Climate change impacts on net primary production (NPP)

W. Fu et al.

1 Introduction

Ocean net primary production (NPP) and particulate organic carbon export (EP) are key elements of marine biogeochemistry and are strongly influenced by warming conditions due to rising concentrations of atmospheric CO_2 and other greenhouse gases. Ocean warming has increasing impacts on ocean ecosystems by modifying the ecophysiology and distribution of marine organisms, and by altering ocean circulation and stratification. Ocean ecosystems also are important components of the climate system, influencing the atmospheric abundance of radiative agents such as CO_2, N_2O, aerosols and the bio-optical properties of seawater and upper ocean physics (Bopp et al., 2013; Goldstein et al., 2003; Manizza et al., 2008; Schmittner and Galbraith, 2008; Siegenthaler and Wenk, 1984). Therefore, understanding the mechanisms controlling NPP and EP is essential for understanding global cycles of carbon and other bioactive elements (Passow and Carlson, 2012).

Upper ocean stratification plays a key role in many ocean biogeochemical processes. In particular, mixed layer depth (MLD) regulates the interplay between light availability for photosynthesis (Hannon et al., 2001) and nutrient supply from the deep to upper oceans (Pollard et al., 2009). Upper ocean stratification is defined here as the density difference between the surface and 200 m depth (Capotondi et al., 2012), which is indicative of the degree of coupling and nutrient fluxes between the euphotic zone and the ocean interior. The density gradient at the base of the mixed layer affects entrainment processes, which play a crucial role in mixed layer deepening and in particle sinking/export from the euphotic zone. Stratification can also influence ocean ventilation (Luo et al., 2009), which has important consequences for oceanic uptake of carbon and oxygen. Thus, changes in stratification over the remainder of the 21st century have the potential to influence NPP and EP across marine ecosystems.

Stratification tends to increase in response to ocean surface warming and freshening. This typically occurs in 21st century global warming simulations as atmospheric greenhouse gas concentrations continue to increase. With sustained increases in

BGD
12, 12851–12897, 2015

warming, many studies document decreases in global NPP and EP (Bopp et al., 2001; Froelicher et al., 2009; Fung et al., 2005; Plattner et al., 2001; Schmittner et al., 2008) using models with varying degrees of complexity. For the RCP8.5 scenario, CMIP5 ESM estimates of changes in export production range from −7 to −18 % relative to 1990s whereas for NPP these changes are smaller, varying from −2 to −16 % (Bopp et al., 2013). Increased stratification reduces the input of sub-surface nutrients to the euphotic zone and can lead to decreasing NPP and EP through increasing nutrient limitation. Increasing nutrient stress also can shift phytoplankton community composition, favoring smaller phytoplankton over larger phytoplankton (Bopp et al., 2001; Steinacher et al., 2010; Vichi et al., 2011; Moore et al., 2013).

The relative importance of different ecological controls on NPP and EP depends, in part, on an individual model's capacity to represent plankton functional types (PFT) (Jin et al., 2006; Le Quere et al., 2005) and their unique physiological and ecological characteristics. For the CMIP5 biogeochemical models, the marine biological cycle is closed in the sense that nutrient uptake by phytoplankton, export of organic material into the thermocline, remineralization of organic material and transport of inorganic nutrients by the circulation are represented. In this regard, these models are suitable to study the response of NPP and EP to stratification changes. However, the treatment of phytoplankton communities is still relatively simple, with most models carrying three or fewer classes (Bopp et al., 2013).

Here we analyze centennial-scale changes in NPP and EP in response to increasing surface stratification and other physical factors. We use historical (1850–2005) and Representative Concentration Pathway (RCP) 8.5 (2006–2100) ESM simulations contributed to the fifth phase of the Coupled Model Inter-comparison Project (CMIP5). One goal of this study is to study long-term trends in NPP and EP under strong warming conditions to identify the mechanisms behind these changes, including the physical factors that regulate nutrient availability. As a part of our analysis, we document how absolute concentrations and fluxes vary across the different models to highlight some

BGD
12, 12851–12897, 2015

of the large differences and considerable uncertainty in the CMIP5 projections of marine biogeochemistry.

2 Methods

We analyzed simulations from a set of 9 ESMs that contributed output to the Earth System Grid Federation as a part of CMIP5 (Taylor et al., 2012). Required physical ocean variables were temperature, salinity, and potential density; required biogeochemistry variables were macro-nutrients (nitrate, phosphate, and silicic acid), iron, chlorophyll, NPP and EP. The selection of the 9 models investigated here (Bentsen et al., 2013; Collins et al., 2011; Doney et al., 2009; Dufresne et al., 2013; Dunne et al., 2013, 2012; Gent et al., 2011; Giorgetta et al., 2013; Ilyina et al., 2013; Jones et al., 2011; Moore et al., 2004; Pahlow and Riebesell, 2000; Seferian et al., 2013; Tjiputra et al., 2013) was based on the availability of the variables necessary for our analysis.

The historical and RCP8.5 simulations we analyzed had prescribed atmospheric CO_2 mole fractions and forcing from other greenhouse gases and aerosols, anthropogenic land use, and solar variability. Volcanic forcing also was included during the historical period. The RCP 8.5 is a strong warming scenario with an increase in radiative forcing of $8.5\,W\,m^{-2}$ by 2100 as atmospheric CO_2 mole fractions reach 936 ppm (Moss et al., 2010; van Vuuren et al., 2011). In the case where several ensemble members were available from an individual ESM, we analyzed only the first member.

A simple description of the 9 ESMs is presented in Tables 1 and 2. Atmospheric and ocean resolutions vary widely across the different models (Table 1). Typical atmospheric horizontal grid resolution is $\sim 2^{\circ}$, but it ranges from 0.94 to 3.8°. Typical ocean horizontal resolution is $\sim 1^{\circ}$, ranging from 0.3 to 2°. In the vertical, there are 24 to 95 levels in the atmosphere and 31 to 63 levels in the ocean. All marine biogeochemical components are nutrient–phytoplankton–zooplankton–detritus (NPZD) models, but with varying degrees of complexity, illustrated for instance by the number of phytoplank-

BGD
12, 12851–12897, 2015

ton functional groups (from 1 to 3) or limiting nutrients (from 3 to 5) that are explicitly represented (Table 2).

In our analysis, we used the CMIP5 variable denoting the vertical integration of NPP and sinking export of organic particles at 100 m (EP). We present global mean estimates as the area-weighted or volume-weighted mean by the grid-cell area/volume from an individual model. Monthly mean data are averaged to obtain annual means and the annual mean data are interpolated onto a common $1^{\circ} \times 1^{\circ}$ regular grid for the comparison of the 2-D fields.

3 Results

3.1 Stratification changes

Stratification, defined here as the density difference between the depth of 200 m and the surface, is a useful indicator of change in the upper ocean, as it integrates changes in both temperature and salinity. In Fig. 1a, we present the time series of global mean stratification changes for the historical period and the RCP8.5 projections. All the models project an increase in stratification (ranging from 6 to 30 % at 2100). However, the amplitude of stratification differs considerably across the models. The GFDL-ESM2M and MPI models are relatively close to the observed mean stratification in the WOA09 dataset (red square, 1.81 kg m^{-3}) for the present era. NorESM1-ME shows the weakest stratification (1.74 kg m^{-3}) while the stratification in HadGEM2-ES is strongest (2.45 kg m^{-3}). Long-term trends are in general agreement across models, but the rate of stratification increase varies, with IPSL-CM5A-MR showing a more rapid increase while NorESM1-ME has the slowest increase in stratification.

Surface processes that decrease density can largely explain the stratification increase in the RCP8.5 projections. Global mean SST warms by 2.6–3.5 °C accompanied by surface salinity decreases of 0.05–0.25 psu over the 21st century (Fig. 1). By 2100, the global mean SST ranges from 20.4 °C (HadGEM2-ES) to 21.8 °C (NorESM1-

BGD
12, 12851–12897, 2015

ME). Model spread decreases in the RCP8.5 projections in response to strong anthropogenic forcing (Fig. 1b). The SSS shows a clear declining tendency from 1850 to 2100 (Fig. 1). Compared to the WOA09 observational data, most of the models are too fresh at the surface in the 1990s, especially the HadGEM2-ES, which has the lowest global mean SSS. The model spread is partly due to internal variability simulated by the climate models. Model differences in spin up procedures, the way RCP scenarios are set up, and the model climate sensitivities all likely contribute to the model spread (Knutti and Hegerl, 2008; Szopa et al., 2013).

Vertical density profiles help to further explain the changes in stratification. Mean vertical profiles of density in the 1990s and the density change between the 1990s and the 2090s show that all the models become more buoyant at the surface as a consequence of heating and/or freshening of the upper ocean (Fig. 2). The density changes at the surface vary by almost a factor of two among models, from $-1.1\,\mathrm{kg\,m^{-3}}$ (HadGEM) to $-0.6\,\mathrm{kg\,m^{-3}}$ (GFDL-ES2M), but converge to a relatively narrow range (approximately $-0.2\,\mathrm{kg\,m^{-3}}$) at 500 m depth. Most of the density changes occur between the surface and 200 m. Below 200 m, the density changes in most of the models vary linearly with depth. Thus, our definition of the stratification index, as the density difference between the surface and 200 m, appears reasonable. The converging reductions in density among models at about 500 m agrees with some previous studies based on observations and CMIP3 data (Bindoff and Willebrand, 2007; Capotondi et al., 2012; Lyman et al., 2010). Compared to WOA09 data, the models generally underestimate the density of surface layer (< 150 m) and most models overestimate the density below 350 m (resulting in a positive stratification bias) (Fig. 2a).

Vertical profiles of temperature and salinity are also shown in Fig. 2. The surface ocean exhibits strong warming of 1.7–3.5 °C by the 2090s and the warming magnitude declines quickly with depth, which is associated with the heat uptake capacity of individual models. For instance, GFDL models seem to be more efficient in transporting heat downward than the IPSL models. Above 300 m, the temperature changes vary widely among the models. Changes in SST as a function of depth are complex, and model-to-

BGD
12, 12851–12897, 2015

model differences may be related to the seasonal thermocline dynamics. At the depth of 500 m, the mean SST change converges at about 1.2 °C. The heat uptake capacity is important because it is linked to ocean diapycnal mixing, and to other processes such as mixing by mesoscale eddies. It is assumed that a model with a weak vertical temperature gradient in the control state has a larger capacity for downward heat transport (Kuhlbrodt and Gregory, 2012). In this study, the heat uptake capacity of GFDL models could be large as the temperature gradients are weaker than other models. The large model spread in temperature profiles suggests considerable differences and uncertainties in the parameterizations of these physical processes across the models. Vertical profiles of salinity are more scattered than for temperature (Fig. 2c). In the 1990s, most of the models underestimate salinity from the surface down to 550 m. Surface salinity is generally biased low by 0.05–0.25 psu. Most of major freshening takes place above 100 m, which helps to increase stratification. Note that the salinity increases at 100–300 m in some models (IPSL, GFDL-ESM2M, HadGEM2-ES) partially compensates the impact of rising temperatures on density.

The relative contribution (%) of temperature change to the stratification change from the 1990s to the 2090s is shown in Fig. 3. Previous studies have shown that salinity contributes significantly to the stratification changes at high latitudes (> 40°) in both hemispheres and in the North Pacific as a consequence of increases in precipitation (Bindoff et al., 2007). From our comparisons, temperature dominates the stratification changes in the tropical and sub-tropical regions (Fig. 3). Salinity dominates the stratification changes in the much of the Arctic Ocean and in the high-latitude North Atlantic.

In some regions the spatial distributions and the driving process differs substantially across models. Generally, the models generally agree well in the tropics and subtropical gyres about the factors driving increasing stratification. In the high latitude North Atlantic, the subpolar Pacific and the western Pacific Ocean, there is poor agreement across the models. In the subtropical gyre of the south Pacific, stratification changes in the IPSL and CESM1-BGC models are more dominated by temperature changes, while the other models exhibit more complicated spatial patterns. In the North Atlantic,

BGD
12, 12851–12897, 2015

salinity contributes more in the IPSL and HadGEM2 models than in other models. The southeastern Pacific is more dominated by salinity in the two GFDL models. In the Southern Ocean, the models show relatively large contributions from both salinity and temperature but with complicated spatial patterns that differ substantially across models. Projections for the regions where the models do not agree even on the driving factor should be viewed with more caution.

The spatial patterns of the changes in stratification are displayed for all the models in Fig. 4. Nearly all the models predict large increases in stratification in the western tropical Pacific, the tropical Indian Ocean, the Arctic Ocean, and in the high latitude North Atlantic (particularly in the Labrador Sea). Our stratification index may underestimate the changes in the high latitude North Atlantic, as the relatively deep mixing in this region means that temperature and salinity at 200 m depth are changing much more rapidly than in other regions. Reductions in the deep winter mixing and NADW formation in this region are a common pattern seen in strong warming climate simulations (i.e. Schwinger et al., 2014). Less drastic increases in stratification are seen over much of the rest of the oceans, with only a few small regions in some models showing decreases in stratification. The one exception is the HadGEM2-ES model which has large stratification reductions in the Arctic (Fig. 4).

3.2 Surface nutrient trends with climate change

One of the key factors determining global NPP is nutrient availability in the euphotic zone. Time series of global mean nutrient (0–100 m) concentrations for nitrate (NO_3), phosphate (PO_4), silicic acid (SiO_4) and dissolved iron (dFe) are presented in Fig. 5. The magnitude of surface nutrient concentrations differs substantially across the models (varying by a factor of ~ 1.5–2, and by a factor of 5 for dissolved iron). The IPSL models have relatively low surface nutrient concentrations. Compared to the WOA09, 2 models overestimate phosphate (CESM1(BGC) and GFDL-ESM2G) and 5 models overestimate nitrate. All of the models overestimate the silicic acid observations, with the exception of CESM1(BGC). The CESM1(BGC) model overestimates surface phosphate concentrations initially, due to excessive nitrogen limitation, but then shows the strongest surface phosphate declines over the 21st century (Fig. 5; Moore et al., 2013).

Over the entire period from 1850–2100, the models all display decreasing trends for surface nitrate, phosphate and silicic acid. Interestingly, surface iron concentrations increase modestly in all but one of the models. Changes in iron concentrations may impact marine productivity, nitrogen fixation rates, and oceanic net CO_2 uptake. In the CMIP5 simulations, iron inputs to the oceans were typically held constant, so the increasing surface concentrations may reflect increasing macronutrient limitation of phytoplankton growth, leading to reduced biological uptake of iron. The reductions in the sinking export flux also reduce the particle scavenging loss term for dissolved iron. In the CESM1-BGC model, increased production in the High Nutrient, Low Chlorophyll (HNLC) regions offset ~ 25 % of the reduction observed in the macronutrient-limited areas with climate change, while changing circulation patterns also altered the lateral transport of iron within the oceans (Moore et al., 2013; Misumi et al., 2014).

The relative changes in nutrient concentrations (0–100 m) (normalized to 1990s means) are presented in Fig. 6. The relative changes in the historical run show a consistent pattern across the models for nitrate, phosphate and dissolved iron (except for HadGEM2-ES). In the RCP8.5 projection, the models show diverging estimates of magnitude of the relative changes. For nitrate, the reductions range between −3 to −14 % and the phosphate changes range between −3 to −20 %. Silicic acid and iron trends are even more variable than for nitrate and phosphate. For silicic acid, there are 3 models showing slight increases, while the others exhibit decreases ranging from ~ 5–17 %. The variability in relative change in silicic acid concentration in the RCP8.5 is likely associated with changes in plankton community and variable diatom production (Bopp et al., 2005). The larger uncertainties in the projections of silicic acid concentrations emphasize the need to improve model representations of phytoplankton community structure in marine ecosystem models (Dutkiewicz et al., 2013). With respect to dissolved iron, the 8 models present an increase of 4–10 % relative to 1990s, while in the NorESM1-ME model surface iron is reduced by 3 %. Pre-industrial levels of iron and silicic acid appear too low for the HadGEM2-ES model (Fig. 6).

In addition to the comparisons of global mean trends, we present the spatial distribution of mean nitrate concentration for the first 100 m (Fig. 7). The CMIP5 models reproduce key observed features of the basin scale distributions of surface nitrate. For example, in the eastern equatorial Pacific, Southern Ocean, subarctic North Atlantic and subarctic Pacific exhibit elevated nitrate concentrations in all the models. In the subtropical gyres of the Atlantic and Pacific basins, the mean nitrate concentration is low. However, inter-model comparisons show some clear disagreements in some key regions. For example, the details of the high-nitrate water distributions vary considerably in the eastern equatorial Pacific. The HNLC condition extends too far north and south of the equator in some models, and too far to the west in others (Fig. 7). The models also differ in intensity and extent of high nitrate concentration waters in the subarctic Pacific, where 6 of 9 models show lower nitrate concentrations than the WOA09 data (MPI-ESM-LR, MPI-ESM-MR and HadGEM2-ES are closer to observations). There are also clear differences in the Arabian Sea and Bay of Bengal, where most models underestimate nitrate concentrations except the GFDL-ESM2M and MPI-ESM-LR models.

Inter-model spread in NPP during the 1990s is pronounced, with NPP as low as 29 $Pg\,C\,yr^{-1}$ (IPSL-CM5A-LR and IPSL-CM5A-MR), while NPP in one model exceeds 75 $Pg\,C\,yr^{-1}$ (GFDL-ESM2M) (Table 3, Fig. 8). Satellite based estimation of NPP is approximately 50 $Pg\,C\,yr^{-1}$ (Behrenfeld et al., 2006; Carr et al., 2006). The MPI-ES-MR and CESM1-BGC models had NPP of 49.8 and 54.2 $Pg\,C\,yr^{-1}$, closer to the satellite-based estimates. The magnitude of EP also differs substantially across models in the 1990s, ranging from 4.4 to 7.2 $Pg\,C\,yr^{-1}$ (Table 3). Seven of the nine models have an EP between 6 and 7.2 $Pg\,C\,yr^{-1}$ in the 1990s, while the HadGEM2-ES and GFDL-ESM2G models had lower EP (< 5 $Pg\,C\,yr^{-1}$).

BGD
12, 12851–12897, 2015

3.3 Climate change impacts on NPP and EP

All of the models exhibit decreasing trends in NPP and EP with climate change, and most models show more rapid decreases during middle to latter part of the 21st century (Figs. 8 and 9, Table 3). All nine models project decreases in export production under RCP8.5 exceeding 5 % relative to levels in the 1990s, whereas the response for NPP is divided into 2 groups after 2020. The CESM1(BGC) and GDFL models experience smaller changes in NPP (< 5 % relative to 1990s) while other models have larger decreases (8–16 %). The largest relative change for NPP is about −16 % (MPI-ESM-LR). The EP decreases range from 7 % (GFDL-ESM2G) to 28 % (IPSL-CM5A-LR). The reductions in global NPP and EP co-vary with increases in stratification (Figs. 1–3). In the 2090s, stratification increases by about 16 % in GFDL-ESM2M and up to 33 % in HadGEM1-ES. The rate of stratification increase is slower in the two GFDL models and CESM1(BGC), which also agrees with the slower rates of relative NPP and EP change.

The variability across models in NPP is substantially larger than that seen in EP (Table 3). The normalized standard deviation was ±27 % for NPP, but only ±12 % for EP in the 1990s. EP is tightly coupled to new nutrient inputs to the euphotic zone in these models. NPP is less tightly coupled as the fraction of regenerated production varies across the models and can vary spatially and temporally within each model. Thus, the large spread in NPP is not mainly a function of the different physical models and their transport of nutrients to the euphotic zone, but rather it is strongly impacted by the export efficiency inherent in the models and the resulting varying levels of regenerated production.

The sinking production flux out of the euphotic zone to net primary production ratio (pe-ratio) is a measure of the export efficiency and also reflects the variable contribution of regenerated production to total NPP (Dugdale and Goering, 1967; Dunne et al., 2007; Eppley and Peterson, 1979). High pe-ratio values are typically associated with productive ecosystems dominated by larger phytoplankton (often diatoms), while low pe-ratios are associated with oligotrophic food webs with most carbon flow

BGD
12, 12851–12897, 2015

through the microbial loop (Pomeroy, 1974; Azam et al., 1983). The CMIP5 models that include both large and small phytoplankton assume higher export efficiency for the large phytoplankton (Moore et al., 2004; Aumont and Bopp, 2006; Seferian et al., 2013; Tjiputra et al., 2013). The fraction of grazed material routed to sinking export is higher by a factor of 3–6 than the fraction routed to sinking export for the small phytoplankton. Diatoms are also very likely to dominate phytoplankton blooms in these models. This drives additional, very efficient, export through aggregation, further enhancing the differences in export efficiency between large and small phytoplankton. Relative to the 1990s, six of the nine models show decreasing trends in the pe-ratio (up to 10 % reduction) (Figs. 8 and 9, Table 3). Diatoms accounted for a smaller percentage of NPP in the 2090s than in the 1990s in all the models, except for the MPI model where nearly all of the production is by the diatoms and the smallest phytoplankton are not explicitly included (Table 3). The declines in pe-ratio and in the percent of NPP by diatoms were modest at the global scale, but larger shifts were seen in some regions (see following sections).

3.4 Increasing stratification and declining nutrients, NPP, and EP

Relative changes in global NPP between the 1990s and the 2090s are plotted against relative change in stratification in Fig. 10a. Across all the ESMs, a good relationship is found with a correlation $r^2 = 0.72$. Larger relative increases in stratification correspond to larger declines in NPP. In addition, the fitted line with a slope of 0.38 separates the models into two groups. In one group (GFDL, IPSL and CESM1-BGC), the NPP reduction is more modest as stratification increases; the other group is composed of the two MPI models, HadGEM1-ES and the NorESM model, which show a more rapid, and fairly linear reduction in NPP with increasing stratification. The reduction of NPP can be partly explained by nutrient changes responding to stratification increases. Across the models, surface nitrate and phosphate concentrations clearly decline as the stratification is enhanced (Fig. 10c and d, with r^2 of 0.80 and 0.82, respectively). The response of surface silicic acid to increasing stratification is much more variable. The

BGD
12, 12851–12897, 2015

projected changes are more divided, as three models (MPI-ESM-LR, MPI-ESM-MR and HadGEM1-ES) show slight increases and the others show reductions in surface silicic acid concentrations (Fig. 10b).

EP is even more closely related to the stratification changes ($R^2 = 0.89$) than NPP (Fig. 10e). The EP change is also closely related to the NPP changes. EP decreases by up to 20 % (Fig. 10e) whereas NPP decreases by 10–18 %. The models display two patterns in terms of the response of NPP and EP to climate change. The first group includes five models (IPSL models, CESM1(BGC) and the GFDL models) where the relative declines in NPP are smaller than the relative declines in EP by a factor of 2 or more (Fig. 9 and Table 3). In this group, the EP drops by about 10 % and the NPP decreases by 5 % or less. In the remaining models the relative declines in EP and NPP are more similar in magnitude. For example, both EP and NPP decrease by about 14 % in the HadGEM2-ES model. The differential declines in NPP and EP in the first group of models documents declining export efficiency for the ocean biological pump, driven by phytoplankton community shifts and a decreased contribution to NPP by large phytoplankton (diatoms) (see below and Figs. 9–13).

Reduced nutrient availability seems to be a major contributor to declines in NPP and EP. However, the relationship varies from one model to another because growth and export are complicated functions of macronutrient limitation, temperature, irradiance and iron limitation, as well as the routing of organic matter within the ecosystem that controls the export efficiency. The NPP response is also strongly impacted by phytoplankton community structure, which modifies export efficiency, and the corresponding magnitude of the regenerated primary production. For the IPSL, CESM1(BGC), and GFDL models that show larger declines in EP than in NPP, this pattern is driven by a decreasing contribution to total NPP by large phytoplankton (Table 3, Figs. 11 and 12). Most of the primary production in these models is by smaller phytoplankton. The GFDL models express this pattern most strongly, with minimal declines in NPP, despite declines in EP approaching 10 % (Fig. 9 and Table 3). The other models tend to have production that is dominated by diatoms, and do not capture the community shifts to-

BGD
12, 12851–12897, 2015

wards increasing small phytoplankton dominance (and reduced export efficiency) under increasing nutrient stress. The declines in NPP with increasing stratification are more linear and more similar in magnitude to the declines in EP (Fig. 10a, b, and h). Thus, there are also very strong correlations between the climate-driven changes in the fractional contribution of diatoms to NPP and both the changes in stratification and the changes in EP (Fig. 10f and g, correlations of $r^2 = 0.85$ and $r^2 = 0.95$, both much higher than the correlation between changing stratification and NPP, $r^2 = 0.71$).

Some of these patterns are illustrated in Fig. 11, which shows the contribution of diatoms (large phytoplankton) to NPP for the 1990s. Most of the models show elevated diatom production at high latitudes and lower diatom contributions in the subtropical gyres. However, there are large discrepancies in the magnitude of the diatom contribution, ranging from about 30 % to more than 90 % in the Arctic Ocean, for example. At the global-scale diatoms account for only 9.4 % of NPP in the GFDL-ESM2M model and reach a maximum of 91 % in the MPI-ESM-MR model (Table 3). The large variability across the models reflects, in part, the lack of an observational dataset to constrain phytoplankton community composition, at the time these models were being developed. The new globally-gridded world ocean atlas of plankton functional types, MAREDAT (Buitenhuis et al., 2013) has started to fill this gap, and will lead to improved representations of plankton community structure in the future as the dataset becomes increasingly populated and is entrained into model development and validation.

The spatial patterns of the shifts in phytoplankton community composition with climate change are illustrated in Fig. 12, where we plot the change in the percent of NPP by diatoms (2090s–1990s). There are some robust trends across the models. One of the areas with the biggest declines in diatom production is the high-latitude North Atlantic. This region typically has some of the biggest stratification increases with climate change, greatly reducing the deep winter mixing that entrains nutrients to the surface (Moore et al., 2013; Schwinger et al., 2014; Randerson et al., 2015). Nearly all the models also show large declines in diatom contributions to production in the Arctic Ocean. The CMIP5 models show consistent trends of increasing stratification, declining surface nutrient concentrations, and a longer growing season with climate change in the Arctic (Vancoppenolle et al., 2013). Increasing surface temperatures and dramatic declines in the sea ice cover allow for a longer growing season with climate change. Thus, nutrients in surface waters are more completely used up by summer's end, leading to community shifts with decreased diatom production and an increased fraction of production by smaller phytoplankton. In the CESM-BGC model, this community shift allows for a small increase in central Arctic NPP, even as export production and surface nutrient concentrations decline, due to the increased fraction of NPP by small phytoplankton and the resulting increase in regenerated production (Moore et al., 2013).

All of the models show some increase in the fraction of NPP by diatoms in the Southern Ocean (Fig. 12). The increase is particularly strong in the CESM1-BGC, IPSL, and GFDL models. Most of the models also show some increased diatom production in the tropical Pacific. Bopp et al. (2005) also found decreasing diatom production in the Arctic and high-latitude North Atlantic, with some increases in the Southern Ocean under a strong warming scenario. Steinacher et al. (2010) also found declining productivity in the North Atlantic, and shifts in the export ratio due to phytoplankton community shifts with decreasing diatom production. The earlier version of the CESM used in that study (CCSM3) showed only small shifts in export ratios with climate change, as the range in export ratios and the differences in export efficiencies between large and small phytoplankton were smaller than in the CESM (Steinacher et al., 2010; Moore et al., 2013). Three models in this study (HadGEM2-ES and the MPI models) show increased diatom production across the low latitudes (Fig. 12). The diatoms dominate production everywhere in these three models (Fig. 11).

There are also large inter-model differences in the spatial patterns of the pe-ratio (Fig. 13). Most of the models (GFDL, IPSL, CESM-BGC) show a close correlation between the pe-ratio and diatom production (compare Figs. 11 and 13), due to the enhanced export efficiency for diatoms (large phytoplankton) built into the models. Thus, there is a very high correlation between the changing contribution of diatoms to NPP

BGD
12, 12851–12897, 2015

and the changes in EP (Fig. 10g, Table 3). The MPI model includes one phytoplankton group and has an essentially constant pe-ratio of 0.15, explaining the linearity of the changes in NPP and EP with warming (Figs. 11 and 13). Production in the HadGEM1-ES model is dominated nearly everywhere by the diatoms (Fig. 11). Therefore, the MPI and HadGEM models cannot capture a shift towards increasing small phytoplankton dominance under declining surface nutrient concentrations. This leads to export production being closely correlated with diatom production in these models as most production is by diatoms, as well as in the other models where diatoms are assumed to export more efficiently but account for a smaller fraction of total NPP (Table 3).

There is also a strong correlation between the declines in the fraction of NPP by diatoms and declines in the pe-ratio (compare Figs. 12 and 14). The largest declines in the pe-ratio are seen in the Arctic and the high-latitude North Atlantic, regions where diatom production also decreased. The GFDL, IPSL, and CESM1(BGC) models also show some reductions in pe-ratio in the subarctic North Pacific, but the spatial patterns are inconsistent (Fig. 14). The models display considerable variability in the degree of stratification increase and in the dominant factor driving these changes in the subarctic North Pacific (Figs. 3 and 4).

The correlation for the relationship between the changing percentage of NPP by diatoms vs. the changes in EP across all the models has an r^2 value of 0.96 and a slope with a value close to 1 (0.94, Fig. 10g) indicating that phytoplankton community structure plays a dominant role in determining the responses of NPP, EP, and the pe-ratio to climate change. The biggest declines in the fraction of production by diatoms and pe-ratios are in precisely the areas where some of the largest increases in upper ocean stratification are seen, along with declining surface nutrient concentrations, as in the Arctic Ocean and in the high latitude North Atlantic (Figs. 9–11; see also Steinacher et al., 2010; Moore et al., 2013).

BGD
12, 12851–12897, 2015
Climate change impacts on net primary production (NPP)
W. Fu et al.

3.5 Projected changes in NPP, EP and stratification biases

At global scale, the CMIP5 models show considerable stratification biases for the 1990s when compared to the WOA09 data (Fig. 2). Only the GFDL-ESM2M model is within 10 % of the observed value (Figs. 2 and 15). From the density profiles, it is apparent that most of the models have stronger stratification in the 1990s than seen in the observations. Liu et al. (2014) argued that climate bias is important when projecting the impact of climate change on land surface processes and Hoffman et al. (2014) documented this for atmospheric CO_2 mole fractions. Here, we examine how stratification biases in the 1990s may affect model projections of NPP and EP in the 2090s.

Models with stronger bias in the 1990s for surface stratification tend to predict larger climate-induced declines in both NPP and EP (Fig. 14, $r^2 = 0.47$ and $r^2 = 0.54$, respectively). Five of the models have positive biases in stratification for the current era that exceed 20 %. These models also show the largest relative increases in stratification with climate change of 26–30 % (Fig. 14, Table 3). The remaining four models (GFDL models, CESM1-BGC, and NorESM1-ME) do a better job of simulating observed stratification for the current era, and predict relative increases in stratification over the 21st century that are roughly half as large, ranging from ~ 15–18 %. This suggests that the more biased models (for the 1990s) may be overestimating the predicted reductions in NPP and EP for the end of the century.

4 Discussion and conclusions

The ESMs analyzed here have different resolutions and incorporate marine biogeochemical-ecosystem models with different mechanisms and degrees of complexity. We find this set of models has consistent trends of increasing stratification and decreasing NPP and EP. However, a large model spread is apparent for the 1990s, particularly for NPP, and in the relative changes to NPP and EP over the 21st century due to climate change. NPP is reduced by 2–18 % in the 2090s and EP is reduced by

7–20 %. Mean stratification increased by 16 % (GFDL-ESM2M) to 33 % (HadGEM1-ES) by the 2090s. Under strong warming scenarios like RCP8.5, ocean stratification will continue increasing after the year 2100 in all of these models.

The strongly linear relationship between stratification increases and EP decreases seen within each model and across all the models (Figs. 10 and 15) indicates a strong bottom up control on EP, through declining nutrient fluxes to the euphotic zone. Declining surface nutrient concentrations are seen in all the models with climate change under the RCP 8.5 scenario (Figs. 5 and 6). Nitrate is reduced by 3 to 14 % and phosphate is reduced by 3 to 20 %. Changes in surface silicic acid and iron concentrations are more variable across the models. For silicic acid, there are 3 models showing slight increases, while the others exhibit decreases of 5–17 %. With respect to iron, 8 models indicate an increase of 4–10 % relative to the 1990s; with the exception being the NorESM1-ME model, which is reduced by 3 %. Changes in the temperature and light fields also have impacts on EP in some regions, but increasing stratification and nutrient stress, and the resulting impacts on phytoplankton community composition and EP is the dominate process at the global scale.

Simulated NPP and its response to climate change are both more variable across the models than EP, and are less strongly correlated with changes in stratification (Fig. 10). This is driven by model differences in the export efficiency of the biological pump and its relation to phytoplankton community structure. The models that allow for shifts in phytoplankton community structure, whereby increasing nutrient stress gives competitive advantage to smaller cells over larger cells, show strongly non-linear responses in NPP to climate change. NPP declines less rapidly than EP with increasing nutrient stress, as the percentage of NPP by large cells declines and export efficiency decreases (and the percentage of regenerated production increases). Models with less dynamic community composition show much more linear NPP response to climate change (Fig. 10). Thus, projections of the response of NPP to climate change in the CMIP5 models are critically dependent on the simulated phytoplankton community structure, the efficiency

BGD
12, 12851–12897, 2015

of the biological pump, and the resulting (highly variable) levels of regenerated production.

The large spread in the simulated NPP rates for the 1990s and the variability seen across models in the response of NPP to climate change introduce challenges for climate impact and risk assessment, as NPP is a key product of both terrestrial and marine ecosystem models, and changes to NPP are perhaps the most cited result from this class of models. We have demonstrated that the wide spread seen in simulated NPP is not due to the different physical circulation models and the flux of nutrients they deliver to surface waters, but rather to the efficiency of the biological pump (tied to community structure in most models) and the resulting levels of regenerated primary production. We suggest that EP may be a more useful proxy of climate impacts on marine systems than changes to NPP. EP is more strongly tied to feedbacks with climate, as it is mainly the fixed carbon sequestered to the deeper ocean by the biological pump that will impact air–sea CO_2 exchange and climate. In addition, in terms of impacts up the food chain, EP is also likely a better proxy. Friedland et al. (2012) show that there is no correlation between fishery yield and NPP at the global scale, but that there are strong correlations between fishery yield and several other variables including chlorophyll concentration, the pe-ratio, and EP. These three proxies all correlate with the fraction of primary production by large phytoplankton. The results presented here suggest future large declines in fishery yield across the high-latitude North Atlantic.

Many of the CMIP5 models have an assumed much higher export efficiency for diatoms relative to small phytoplankton, building on a long-standing paradigm, strengthened by results from the detailed ecosystem studies of the Joint Global Flux Study (JGOFS) program (Boyd and Newton, 1999; Buesseler, 1998). In the current models, the spectrum of phytoplankton size structure is often represented very simply with only the end members of one large and one small phytoplankton group. Thus, the "diatom" group is a proxy for all the larger, efficiently exporting, blooming phytoplankton. DOM cycling, heterotrophic bacteria, microzooplankton, and the microbial loop are typically treated in an idealized, implicit manner in the current models as well.

BGD
12, 12851–12897, 2015

To accurately predict the response of NPP and EP to climate change, it may be necessary to develop more robust ecosystem models with additional explicit phytoplankton, heterotrophic microbial, and zooplankton groups, including their impacts on nutrient cycling, export efficiency and the downward transport of organic matter. Some models that include much greater diversity in the phytoplankton, show large community composition shifts with climate change (Dutkiewicz et al., 2013). Quantifying the links between NPP, EP and community composition should be a high priority. There are only limited field observations of the pe-ratio, some of which rely on nutrient drawdown and other indirect estimates of the sinking particle flux (Dunne et al., 2007). Further progress to improve model performance requires combined efforts from satellite, field, and laboratory observations, empirical and inverse modeling approaches, as well as process-based, forward models.

The large model spread in EP and NPP, and significant biases seen in key nutrient fields for the 1990s suggest that the current ocean biogeochemical models are far from perfect and their results must be interpreted with some caution. However, the relationships between stratification and EP, NPP and nutrients do reveal some common mechanisms driving the climate change response. The large inter-model differences for the current era in NPP, EP and nutrient concentrations are partially associated with how these biogeochemical models are initialized and spun up for these experiments. The ocean biogeochemical model is usually integrated in an offline mode for a thousand years or more before coupling to other components of the ESM. The achieved near-steady state of biogeochemical fields may deviate substantially from the observed climatology, driven by biases in the physics and biogeochemistry. These differences typically persist in the present-day simulations and future projections. The advantage of the initialization and spin up process is that the biogeochemical fields are consistent with the simulated ocean circulation, and will respond to climate-driven changes appropriately. The strong intrinsic variability helps to reduce model drift and generate reasonable longer-term variability. As a result, these long-term simulations are suitable for analyzing climate trends, variability and sensitivities. RCP 8.5 is a strong warm-

BGD
12, 12851–12897, 2015

ing scenario and the relationship between stratification changes and NPP/EP changes may be somewhat different under other RCP scenarios. Although the relations between the degree of surface warming and the ocean biogeochemical responses were largely linear across RCP 4.5 and 8.5 for the CESM(BGC) (Moore et al., 2013).

Some potentially important marine biogeochemical feedbacks on the climate system were not well represented in the CMIP5 models, including important feedbacks through aerosol transport and deposition on the marine iron cycle, feedbacks involving the oxygen minimum zones and the marine nitrogen cycle, and the impacts on biology by the ongoing ocean acidification. Each of these feedbacks could impact phytoplankton and zooplankton community structures, NPP, EP, and pe-ratios in the future.

It is also important to consider the longer-term climate change responses of both ocean physics and marine biogeochemistry. Moore et al. (2013) noted that climate impacts on the oceans were still accelerating at year 2100 under the RCP 8.5 scenario (but not under the more moderate RCP 4.5 scenario). Randerson et al. (2015) extended the CESM1(BGC) RCP 8.5 scenario simulation examined here, out to the year 2300. In these longer simulations, the climate impacts on ocean physical fields and biogeochemistry lead to even stronger perturbations after 2100 than those presented here for the 2090s. In addition, the ocean contribution to the climate-carbon feedback exceeded the land contribution after the year 2100 (Randerson et al., 2015).

Acknowledgements. We are grateful for support from the US Dept. of Energy Office of Science and the National Science Foundation (NSF). This contribution was supported by a grant to UCI as a part of the BGC Feedbacks Scientific Focus Area within the Regional and Global Climate Modeling (RGCM) Program in the Climate and Environmental Sciences Division (CESD) of the Biological and Environmental Research (BER) Program in the US Dept. of Energy Office of Science. We also received funding from the NSF project "Collaborative Research: Improved Regional and Decadal Predictions of the Carbon Cycle" (AGS-1048890). We would also like to thank all those in the CMIP5 project efforts, which made this work possible.

References

Aumont, O. and Bopp, L.: Globalizing results from ocean in situ iron fertilization studies, Global Biogeochem. Cy., 20, GB2017, doi:2010.1029/2005GB002591, 2006.

Azam, F., Fenchel, T., Field, J. G., Gray, J. S., Meyerreil, L. A., and Thingstad, F.: The ecological role of water-column microbes in the sea, Mar. Ecol.-Prog. Ser., 10, 257–263, 1983.

Behrenfeld, M. J., O'Malley, R. T., Siegel, D. A., McClain, C. R., Sarmiento, J. L., Feldman, G. C., Milligan, A. J., Falkowski, P. G., Letelier, R. M., and Boss, E. S.: Climate-driven trends in contemporary ocean productivity, Nature, 444, 752–755, 2006.

Bentsen, M., Bethke, I., Debernard, J. B., Iversen, T., Kirkevåg, A., Seland, Ø., Drange, H., Roelandt, C., Seierstad, I. A., Hoose, C., and Kristjánsson, J. E.: The Norwegian Earth System Model, NorESM1-M – Part 1: Description and basic evaluation of the physical climate, Geosci. Model Dev., 6, 687–720, doi:10.5194/gmd-6-687-2013, 2013.

Bindoff, N. L. and Willebrand, J.: Observations: Oceanic Climate Change and Sea Level, Cambridge University Press, Cambridge, 385–432, 2007.

Booth, B. B. B., Bernie, D., McNeall, D., Hawkins, E., Caesar, J., Boulton, C., Friedlingstein, P., and Sexton, D. M. H.: Scenario and modelling uncertainty in global mean temperature change derived from emission-driven global climate models, Earth Syst. Dynam., 4, 95–108, doi:10.5194/esd-4-95-2013, 2013.

Bopp, L., Monfray, P., Aumont, O., Dufresne, J. L., Le Treut, H., Madec, G., Terray, L., and Orr, J. C.: Potential impact of climate change on marine export production, Global Biogeochem. Cy., 15, 81–99, 2001.

Bopp, L., Aumont, O., Cadule, P., Alvain, S., and Gehlen, M.: Response of diatoms distribution to global warming and potential implications: a global model study, Geophys. Res. Lett., 32, L19606, doi:19610.11029/12005gl023653, 2005.

Bopp, L., Resplandy, L., Orr, J. C., Doney, S. C., Dunne, J. P., Gehlen, M., Halloran, P., Heinze, C., Ilyina, T., Séférian, R., Tjiputra, J., and Vichi, M.: Multiple stressors of ocean ecosystems in the 21st century: projections with CMIP5 models, Biogeosciences, 10, 6225–6245, doi:10.5194/bg-10-6225-2013, 2013.

Boyd, P. W. and Newton, P. P.: Does planktonic community structure determine downward particulate organic carbon flux in different oceanic provinces?, Deep-Sea Res. Pt. I, 46, 63–91, 1999.

BGD
12, 12851–12897, 2015

Climate change impacts on net primary production (NPP)

W. Fu et al.

Buesseler, K. O.: The decoupling of production and particulate export in the surface ocean, Global Biogeochem. Cy., 12, 297–310, 1998.
Buitenhuis, E. T., Vogt, M., Moriarty, R., Bednaršek, N., Doney, S. C., Leblanc, K., Le Quéré, C., Luo, Y.-W., O'Brien, C., O'Brien, T., Peloquin, J., Schiebel, R., and Swan, C.: MAREDAT: towards a world atlas of MARine Ecosystem DATa, Earth Syst. Sci. Data, 5, 227–239, doi:10.5194/essd-5-227-2013, 2013.
Capotondi, A., Alexander, M. A., Bond, N. A., Curchitser, E. N., and Scott, J. D.: Enhanced upper ocean stratification with climate change in the CMIP3 models, J. Geophys. Res.-Oceans, 117, C04031, doi:04010.01029/02011JC007409, 2012.
Carr, M. E., Friedrichs, M. A. M., Schmeltz, M., Aita, M. N., Antoine, D., Arrigo, K. R., Asanuma, I., Aumont, O., Barber, R., Behrenfeld, M., Bidigare, R., Buitenhuis, E. T., Campbell, J., Ciotti, A., Dierssen, H., Dowell, M., Dunne, J., Esaias, W., Gentili, B., Gregg, W., Groom, S., Hoepffner, N., Ishizaka, J., Kameda, T., Le Quere, C., Lohrenz, S., Marra, J., Melin, F., Moore, K., Morel, A., Reddy, T. E., Ryan, J., Scardi, M., Smyth, T., Turpie, K., Tilstone, G., Waters, K., and Yamanaka, Y.: A comparison of global estimates of marine primary production from ocean color, Deep-Sea Res. Pt. II, 53, 741–770, 2006.
Collins, W. J., Bellouin, N., Doutriaux-Boucher, M., Gedney, N., Halloran, P., Hinton, T., Hughes, J., Jones, C. D., Joshi, M., Liddicoat, S., Martin, G., O'Connor, F., Rae, J., Senior, C., Sitch, S., Totterdell, I., Wiltshire, A., and Woodward, S.: Development and evaluation of an Earth-System model – HadGEM2, Geosci. Model Dev., 4, 1051–1075, doi:10.5194/gmd-4-1051-2011, 2011.
Doney, S. C., Lima, I., Feely, R. A., Glover, D. M., Lindsay, K., Mahowald, N., Moore, J. K., and Wanninkhof, R.: Mechanisms governing interannual variability in upper-ocean inorganic carbon system and air–sea CO_2 fluxes: physical climate and atmospheric dust, Deep-Sea Res. Pt. II, 56, 640–655, 2009.
Dufresne, J. L., Foujols, M. A., Denvil, S., Caubel, A., Marti, O., Aumont, O., Balkanski, Y., Bekki, S., Bellenger, H., Benshila, R., Bony, S., Bopp, L., Braconnot, P., Brockmann, P., Cadule, P., Cheruy, F., Codron, F., Cozic, A., Cugnet, D., de Noblet, N., Duvel, J. P., Ethe, C., Fairhead, L., Fichefet, T., Flavoni, S., Friedlingstein, P., Grandpeix, J. Y., Guez, L., Guilyardi, E., Hauglustaine, D., Hourdin, F., Idelkadi, A., Ghattas, J., Joussaume, S., Kageyama, M., Krinner, G., Labetoulle, S., Lahellec, A., Lefebvre, M. P., Lefevre, F., Levy, C., Li, Z. X., Lloyd, J., Lott, F., Madec, G., Mancip, M., Marchand, M., Masson, S., Meurdesoif, Y., Mignot, J., Musat, I., Parouty, S., Polcher, J., Rio, C., Schulz, M., Swingedouw, D., Szopa, S., Talandier,

BGD
12, 12851–12897, 2015

Climate change impacts on net primary production (NPP)

W. Fu et al.

C., Terray, P., Viovy, N., and Vuichard, N.: Climate change projections using the IPSL-CM5 Earth System Model: from CMIP3 to CMIP5, Clim. Dynam., 40, 2123–2165, 2013.
Dugdale, R. C. and Goering, J. J.: Uptake of new and regenerated forms of nitrogen in primary productivity, Limnol. Oceanogr., 12, 196–206, 1967.
Dunne, J. P., Sarmiento, J. L., and Gnanadesikan, A.: A synthesis of global particle export from the surface ocean and cycling through the ocean interior and on the seafloor, Global Biogeochem. Cy., 21, Gb4006, doi:10.1029/2006gb002907, 2007.
Dunne, J. P., John, J. G., Adcroft, A. J., Griffies, S. M., Hallberg, R. W., Shevliakova, E., Stouffer, R. J., Cooke, W., Dunne, K. A., Harrison, M. J., Krasting, J. P., Malyshev, S. L., Milly, P. C. D., Phillipps, P. J., Sentman, L. T., Samuels, B. L., Spelman, M. J., Winton, M., W ittenberg, A. T., and Zadeh, N.: GFDL's ESM2 global coupled climate-carbon earth system models. Part I: Physical formulation and baseline simulation characteristics, J. Climate, 25, 6646–6665, 2012.
Dunne, J. P., John, J. G., Shevliakova, E., Stouffer, R. J., Krasting, J. P., Malyshev, S. L., Milly, P. C. D., Sentman, L. T., Adcroft, A. J., Cooke, W., Dunne, K. A., Griffies, S. M., Hallberg, R. W., Harrison, M. J., Levy, H., Wittenberg, A. T., Phillips, P. J., and Zadeh, N.: GFDL's ESM2 global coupled climate-carbon earth system models. Part II: Carbon system formulation and baseline simulation characteristics, J. Climate, 26, 2247–2267, 2013.
Dutkiewicz, S., Scott, J. R., and Follows, M. J.: Winners and losers: ecological and biogeochemical changes in a warming ocean, Global Biogeochem. Cy., 27, 463–477, 2013.
Eppley, R. W. and Peterson, B. J.: Particulate organic-matter flux and planktonic new production in the deep ocean, Nature, 282, 677–680, 1979.
Friedland, K. D., Stock, C., Drinkwater, K. F., Link, J. S., Leaf, R. T., Shank, B. V., Rose, J. M., Pilskaln, C. H., and Fogarty, M. J.: Pathways between primary production and fisheries yields of large marine ecosystems, PLoS One, 7, e28945, doi:10.1371/journal.pone.0028945, 2012.
Friedlingstein, P., Meinshausen, M., Arora, V. K., Jones, C. D., Anav, A., Liddicoat, S. K., and Knutti, R.: Uncertainties in CMIP5 climate projections due to carbon cycle feedbacks, J. Climate, 27, 511–526, 2014.
Froelicher, T. L., Joos, F., Plattner, G. K., Steinacher, M., and Doney, S. C.: Natural variability and anthropogenic trends in oceanic oxygen in a coupled carbon cycle-climate model ensemble, Global Biogeochem. Cy., 23, Gb1003, doi:1010.1029/2008gb003316, 2009.
Fung, I. Y., Doney, S. C., Lindsay, K., and John, J.: Evolution of carbon sinks in a changing climate, P. Natl. Acad. Sci. USA, 102, 11201–11206, 2005.

BGD
12, 12851–12897, 2015

Gent, P. R., Danabasoglu, G., Donner, L. J., Holland, M. M., Hunke, E. C., Jayne, S. R., Lawrence, D. M., Neale, R. B., Rasch, P. J., Vertenstein, M., Worley, P. H., Yang, Z.-L., and Zhang, M.: The community climate system model version 4, J. Climate, 24, 4973–4991, 2011.

Giorgetta, M. A., Jungclaus, J., Reick, C. H., Legutke, S., Bader, J., Böttinger, M., Brovkin, V., Crueger, T., Esch, M., and Fieg, K.: Climate and carbon cycle changes from 1850 to 2100 in MPI-ESM simulations for the coupled model intercomparison project phase 5, J. Adv. Model. Earth Sy., 5, 572–597, 2013.

Goldstein, B., Joos, F., and Stocker, T. F.: A modeling study of oceanic nitrous oxide during the Younger Dryas cold period, Geophys. Res. Lett., 30, 1092, doi: 1092, doi:10.1029/2002gl016418, 2003.

Hannon, E., Boyd, P. W., Silvoso, M., and Lancelot, C.: Modeling the bloom evolution and carbon flows during SOIREE: implications for future in situ iron-enrichments in the Southern Ocean, Deep-Sea Res. Pt. II, 48, 2745–2773, 2001.

Ilyina, T., Six, K. D., Segschneider, J., Maier-Reimer, E., Li, H., and Núñez-Riboni, I.: Global ocean biogeochemistry model HAMOCC: model architecture and performance as component of the MPI-Earth system model in different CMIP5 experimental realizations, J. Adv. Model. Earth Sy., 5, 287–315, 2013.

Jin, X., Gruber, N., Dunne, J. P., Sarmiento, J. L., and Armstrong, R. A.: Diagnosing the contribution of phytoplankton functional groups to the production and export of particulate organic carbon, $CaCO_3$, and opal from global nutrient and alkalinity distributions, Global Biogeochem. Cy., 20, Gb2015, doi:10.1029/2005gb002532, 2006.

Jones, C. D., Hughes, J. K., Bellouin, N., Hardiman, S. C., Jones, G. S., Knight, J., Liddicoat, S., O'Connor, F. M., Andres, R. J., Bell, C., Boo, K.-O., Bozzo, A., Butchart, N., Cadule, P., Corbin, K. D., Doutriaux-Boucher, M., Friedlingstein, P., Gornall, J., Gray, L., Halloran, P. R., Hurtt, G., Ingram, W. J., Lamarque, J.-F., Law, R. M., Meinshausen, M., Osprey, S., Palin, E. J., Parsons Chini, L., Raddatz, T., Sanderson, M. G., Sellar, A. A., Schurer, A., Valdes, P., Wood, N., Woodward, S., Yoshioka, M., and Zerroukat, M.: The HadGEM2-ES implementation of CMIP5 centennial simulations, Geosci. Model Dev., 4, 543–570, doi:10.5194/gmd-4-543-2011, 2011.

Jones, C., Hughes, J., Bellouin, N., Hardiman, S., Jones, G., Knight, J., Liddicoat, S., O'Connor, F., Andres, R. J., and Bell, C.: Twenty-first-century compatible CO_2 emissions and airborne

fraction simulated by CMIP5 earth system models under four representative concentration pathways, J. Climate, 26, 4398–4413, 2013.
Knutti, R. and Hegerl, G. C.: The equilibrium sensitivity of the Earth's temperature to radiation changes, Nat. Geosci., 1, 735–743, 2008.
Kuhlbrodt, T. and Gregory, J. M.: Ocean heat uptake and its consequences for the magnitude of sea level rise and climate change, Geophys. Res. Lett., 39, L18608, doi:10.11029/12012GL052952, 2012.
Le Quere, C., Harrison, S. P., Prentice, I. C., Buitenhuis, E. T., Aumont, O., Bopp, L., Claustre, H., Da Cunha, L. C., Geider, R., Giraud, X., Klaas, C., Kohfeld, K. E., Legendre, L., Manizza, M., Platt, T., Rivkin, R. B., Sathyendranath, S., Uitz, J., Watson, A. J., and Wolf-Gladrow, D.: Ecosystem dynamics based on plankton functional types for global ocean biogeochemistry models, Glob. Change Biol., 11, 2016–2040, 2005.
Liu, M., Rajagopalan, K., Chung, S. H., Jiang, X., Harrison, J., Nergui, T., Guenther, A., Miller, C., Reyes, J., Tague, C., Choate, J., Salathé, E. P., Stöckle, C. O., and Adam, J. C.: What is the importance of climate model bias when projecting the impacts of climate change on land surface processes?, Biogeosciences, 11, 2601–2622, doi:10.5194/bg-11-2601-2014, 2014.
Luo, Y. Y., Liu, Q. Y., and Rothstein, L. M.: Simulated response of North Pacific Mode Waters to global warming, Geophys. Res. Lett., 36, L23609, doi:23610.21029/22009gl040906, 2009.
Lyman, J. M., Good, S. A., Gouretski, V. V., Ishii, M., Johnson, G. C., Palmer, M. D., Smith, D. M., and Willis, J. K.: Robust warming of the global upper ocean, Nature, 465, 334–337, 2010.
Manizza, M., Le Quere, C., Watson, A. J., and Buitenhuis, E. T.: Ocean biogeochemical response to phytoplankton-light feedback in a global model, J. Geophys. Res.-Oceans, 113, C10010, doi:10.11029/12007jc004478, 2008.
Misumi, K., Lindsay, K., Moore, J. K., Doney, S. C., Bryan, F. O., Tsumune, D., and Yoshida, Y.: The iron budget in ocean surface waters in the 20th and 21st centuries: projections by the Community Earth System Model version 1, Biogeosciences, 11, 33–55, doi:10.5194/bg-11-33-2014, 2014.
Moore, J., Lindsay, K., Doney, S., Long, M., and Misumi, K.: Marine Ecosystem Dynamics and Biogeochemical Cycling in the Community Earth System Model [CESM1(BGC)]: comparison of the 1990s with the 2090s under the RCP4.5 and RCP8.5 Scenarios, J. Climate, 26, 9291–9312, 2013.

BGD
12, 12851–12897, 2015
Climate change impacts on net primary production (NPP)
W. Fu et al.

Moore, J. K., Doney, S. C., and Lindsay, K.: Upper ocean ecosystem dynamics and iron cycling in a global three-dimensional model, Global Biogeochem. Cy., 18, GB4028, doi:10.1029/2004gb002220, 2004.

Moss, R. H., Edmonds, J. A., Hibbard, K. A., Manning, M. R., Rose, S. K., van Vuuren, D. P., Carter, T. R., Emori, S., Kainuma, M., Kram, T., Meehl, G. A., Mitchell, J. F. B., Nakicenovic, N., Riahi, K., Smith, S. J., Stouffer, R. J., Thomson, A. M., Weyant, J. P., and Wilbanks, T. J.: The next generation of scenarios for climate change research and assessment, Nature, 463, 747–756, 2010.

Pahlow, M. and Riebesell, U.: Temporal trends in deep ocean Redfield ratios, Science, 287, 831–833, 2000.

Passow, U. and Carlson, C. A.: The biological pump in a high CO_2 world, Mar. Ecol.-Prog. Ser., 470, 249–271, 2012.

Plattner, G. K., Joos, F., Stocker, T. F., and Marchal, O.: Feedback mechanisms and sensitivities of ocean carbon uptake under global warming, Tellus B, 53, 564–592, 2001.

Pollard, R. T., Salter, I., Sanders, R. J., Lucas, M. I., Moore, C. M., Mills, R. A., Statham, P. J., Allen, J. T., Baker, A. R., Bakker, D. C., Charette, M. A., Fielding, S., Fones, G. R., French, M., Hickman, A. E., Holland, R. J., Hughes, J. A., Jickells, T. D., Lampitt, R. S., Morris, P. J., Nedelec, F. H., Nielsdottir, M., Planquette, H., Popova, E. E., Poulton, A. J., Read, J. F., Seeyave, S., Smith, T., Stinchcombe, M., Taylor, S., Thomalla, S., Venables, H. J., Williamson, R., and Zubkov, M. V.: Southern Ocean deep-water carbon export enhanced by natural iron fertilization, Nature, 457, 577–581, 2009.

Pomeroy, L. R.: The ocean's food web, a changing paradigm, Bioscience, 24, 499–504, 1974.

Randerson, J., Lindsay, K., Munoz, E., Fu, W., Moore, J., Hoffman, F., Mahowald, N., and Doney, S.: Multi?century changes in ocean and land contributions to climate carbon feedbacks, Global Biogeochem. Cy., 29, 744–759, 2015.

Schmittner, A. and Galbraith, E. D.: Glacial greenhouse-gas fluctuations controlled by ocean circulation changes, Nature, 456, 373–376, 2008.

Schmittner, A., Oschlies, A., Matthews, H. D., and Galbraith, E. D.: Future changes in climate, ocean circulation, ecosystems, and biogeochemical cycling simulated for a business-as-usual CO_2 emission scenario until year 4000 AD, Global Biogeochem. Cy., 22, Gb1013, doi:1010.1029/2007gb002953, 2008.

Seferian, R., Bopp, L., Gehlen, M., Orr, J. C., Ethe, C., Cadule, P., Aumont, O., Salas y Melia, D., Voldoire, A., and Madec, G.: Skill assessment of three earth system models with common marine biogeochemistry, Clim. Dynam., 40, 2549–2573, 2013.
Siegenthaler, U. and Wenk, T.: Rapid atmospheric CO_2 variations and ocean circulation, Nature, 308, 624–626, 1984.
Steinacher, M., Joos, F., Frölicher, T. L., Bopp, L., Cadule, P., Cocco, V., Doney, S. C., Gehlen, M., Lindsay, K., Moore, J. K., Schneider, B., and Segschneider, J.: Projected 21st century decrease in marine productivity: a multi-model analysis, Biogeosciences, 7, 979–1005, doi:10.5194/bg-7-979-2010, 2010.
Szopa, S., Balkanski, Y., Schulz, M., Bekki, S., Cugnet, D., Fortems-Cheiney, A., Turquety, S., Cozic, A., Deandreis, C., Hauglustaine, D., Idelkadi, A., Lathiere, J., Lefevre, F., Marchand, M., Vuolo, R., Yan, N., and Dufresne, J. L.: Aerosol and ozone changes as forcing for climate evolution between 1850 and 2100, Clim. Dynam., 40, 2223–2250, 2013.
Taylor, K. E., Stouffer, R. J., and Meehl, G. A.: An overview of cmip5 and the experiment design, B. Am. Meteorol. Soc., 93, 485–498, 2012.
Tjiputra, J. F., Roelandt, C., Bentsen, M., Lawrence, D. M., Lorentzen, T., Schwinger, J., Seland, Ø., and Heinze, C.: Evaluation of the carbon cycle components in the Norwegian Earth System Model (NorESM), Geosci. Model Dev., 6, 301–325, doi:10.5194/gmd-6-301-2013, 2013.
van Vuuren, D. P., Edmonds, J., Kainuma, M., Riahi, K., Thomson, A., Hibbard, K., Hurtt, G. C., Kram, T., Krey, V., Lamarque, J.-F., Masui, T., Meinshausen, M., Nakicenovic, N., Smith, S. J., and Rose, S. K.: The representative concentration pathways: an overview, Climatic Change, 109, 5–31, 2011.
Vancoppenolle, M., Bopp, L., Madec, G., Dunne, J., Ilyina, T., Halloran, P. R., and Steiner, N.: Future Arctic Ocean primary productivity from CMIP5 simulations: uncertain outcome, but consistent mechanisms, Global Biogeochem. Cy., 27, 605–619, 2013.
Vichi, M., Manzini, E., Fogli, P. G., Alessandri, A., Patara, L., Scoccimarro, E., Masina, S., and Navarra, A.: Global and regional ocean carbon uptake and climate change: sensitivity to a substantial mitigation scenario, Clim. Dynam., 37, 1929–1947, 2011.

Table 1. A brief description of components of the ESMs used in this study, for atmosphere and ocean components, the number of levels in the vertical is indicated by "lev" and then the horizontal resolution is indicated in degrees, vertical coordinates of the ocean and biogeochemical components are indicated by Z (geopotential) or I (isopycnal).

Model	Resolution Atmosphere	Resolution Ocean	Vertical coordinate	Reference	Biogeochemical component	References
GFDL-ES2M	24 lev, 2.5/2.0°	50 lev, 0, 3–1°	Z	Dunne et al. (2013a)	TOPAZ2	Dunne et al. (2013b)
GFDL-ES2G	24 lev, 2.5/2.0°	50 lev, 0, 3–1°	Z + I	Dunne et al. (2013a)	TOPAZ2	Dunne et al. (2013b)
MPI-ESM-LR	47 lev, 1.9°	40 lev, 1.5°	Z	Giorgetta et al. (2013)	HAMOCC5.2	Ilyina et al. (2013)
MPI-ESM-MR	47 lev, 1.9°	40 lev, 0.4°	Z	Giorgetta et al. (2013)	HAMOCC5.2	Ilyina et al. (2013)
IPSL-CM5A-LR	39 lev, 1.9/3.8°	31 lev, 0.5–2°	I	Dufresne et al. (2013)	PISCES	Aumont and Bopp (2006)
IPSL-CM5A-MR	39 lev, 1.2/1.9°	31 lev, 0.5–2°	I	Dufresne et al. (2013)	PISCES	Aumont and Bopp (2006) Seferian et al. (2013)
HadGEM2-ES	38 lev, 1.2/1.9°	40 lev, 0.3–1°	Z	Jones et al. (2011) Collins et al. (2011)	Diat-HadOCC	Palmer and Totterdell (2000)
CESM-BGC	26 lev, 1.25/0.94°	60 lev, 1.125° /0.27–0.53°	Z	Gent et al. (2011) Lindsay et al. (2013)	BEC	Moore et al. (2004) Doney et al. (2009)
NorESM1-ME	26 lev, 1.9°	70 lev, 1.5°	I	Bentsen et al. (2013)	HAMOCC5.1	Tjiputra et al. (2013)

Table 2. A brief description of the marine biogeochemical components included in the ESMs. Nutrients limiting phytoplankton growth, the number of explicit phytoplankton groups, the number of explicit zooplankton groups, representation of heterotrophic bacteria, the use of fixed (Redfield: R) or variable (V) ratios for organic matter production, and Q_{10} for temperature dependency of biogeochemical processes (autotrophic/heterotrophic) are indicated.

Model	Nutrients	Phytoplankton	Zooplankton	Organic Materia Ratio	Q_{10}
TOPAZ2	5 (NO_3, NH_4, PO_4, SiO_4, F_e)	3 (diatom, eukaryotes, small diazotrophs)	1	R(C:N) V(P, S_i, Chl, F_e)	1.88
HAMOCC5.2	3 (NO_3, F_e, PO_4)	1 (separated into, diatoms and calcifiers)	1	R(C:N:P:F_e)	1.88
HAMOCC5.1	3 (NO_3, F_e, PO_4)	1 (separated into, diatoms and calcifiers)	1	R(C:N:P:F_e)	1.88
PISCES	5 (NO_3, F_e, PO_4, NH_4, SiO_4	2 (diatoms and, nanophytoplankton)	2 (micro and meso-)	R(C:N:P) V(S_i, Chl, F_e)	1.88/2.14
Diat-HadOCC	4 (NO_3, F_e, NH_4, SiO_4	2 (diatoms and, non-diatom)	1	R(C:N) V(S_i, F_e)	none
BEC	5 (NO_3, NH_4, PO_4, SiO_4, F_e)	3 (diatom, nano-, phyto, diazotrophy)	1	R(C:N:P) V(S_i, Chl, F_e)	2.0

BGD
12, 12851–12897, 2015

Table 3. Global average of sea surface temperature (SST), sea surface salinity (SSS), nitrate (NO_3), phosphate (PO_4), NPP, EP, particle export ratio (pe-ratio), stratification index (SI) defined as density difference between 200 m and the surface and NPP by diatom (%) for the 1990s and 2090s. Observed estimates for the 1990s are obtained from WOA09 data for SST, SSS, nitrate and phosphate, from Carr et al. (2006) for NPP.

	SST °C		SSS psu		NO_3 (0–100 m) mmol m^{-3}		PO_4 (0–100 m) mmol m^{-3}		NPP Pg C yr^{-1}		EP Pg C yr^{-1}		pe-ratio %		SI kg m^{-3}		%Diat %	
	1990s	2090s	1990s	2090s	1990s	2090s	1990s	2090s	1990s	2090s	1990s	2090s	1990s	2090s	1990s	2090s	1990s	2090s
Observations	18.3		34.57		6.73		0.63		50.0						1.81			
GFDL-ESM2G	18.5	20.4	34.06	33.98	6.65	6.10	0.66	0.58	57.8	57.5	4.40	4.10	7.60	7.02	2.35	2.75	10.7	9.7
GFDL-ESM2M	18.8	20.6	34.32	34.24	8.67	8.22	0.58	0.55	77.6	78.1	6.54	6.06	8.44	7.77	1.95	2.31	9.4	8.8
MPI-ESM-LR	18.3	20.7	34.38	34.23	7.20	6.61	0.57	0.50	45.7	41.6	7.23	6.05	15.84	14.56	1.88	2.41	78.7	80.1
MPI-ESM-MR	18.4	20.9	34.41	34.25	6.96	6.45	0.53	0.47	47.9	43.0	6.56	5.67	13.70	13.20	1.97	2.50	91.1	92.2
IPSL-CM5A-LR	17.7	21.0	34.52	34.43	5.62	4.81	0.43	0.36	28.9	27.0	5.96	4.87	20.61	18.05	2.05	2.63	23.1	20.3
IPSL-CM5A-MR	18.2	21.5	34.42	34.33	5.82	4.99	0.45	0.38	31.8	29.3	6.33	5.28	19.94	17.99	2.12	2.75	22.0	19.7
HadGEM2-ES	18.3	21.5	34.06	33.83	6.56	5.82	0.44	0.36	34.5	29.7	4.77	4.10	13.82	13.79	2.45	3.18	58.8	58.3
CESM1-BGC	19.0	21.4	34.23	34.18	7.60	6.56	0.71	0.54	54.2	52.1	6.97	6.26	12.86	12.03	2.25	2.63	35.7	33.2
NorESM1-ME	18.1	20.2	34.34	34.26	7.01	6.18	0.60	0.51	38.6	35.3	6.81	6.18	17.64	17.52	1.74	2.01		
Model Mean	18.4	20.9	34.30	34.19	6.90	6.19	0.55	0.47	46.3	43.7	6.17	5.39	14.49	13.55	2.08	2.57	41.2	40.3

BGD
12, 12851–12897, 2015
Climate change impacts on net primary production (NPP)
W. Fu et al.

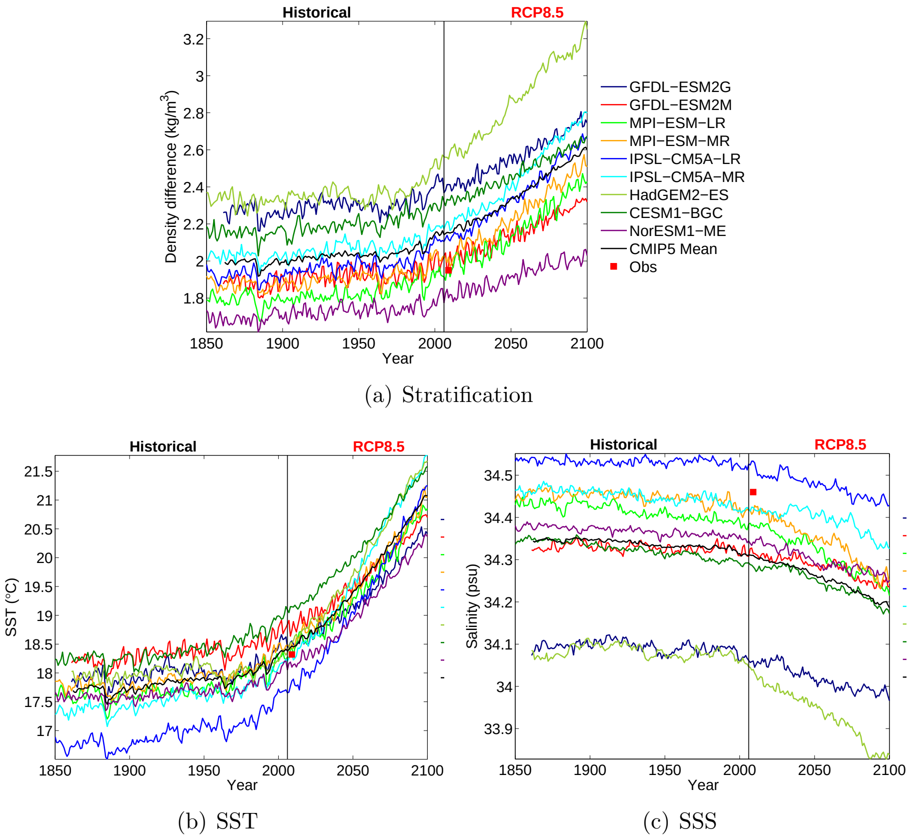

Figure 1. Time series of global mean surface stratification, SST and SSS for historical run and RCP8.5 over 1850–2100. Surface stratification is defined as the density difference between 200 m and the surface. Red square indicates observations from the WOA2009 data.

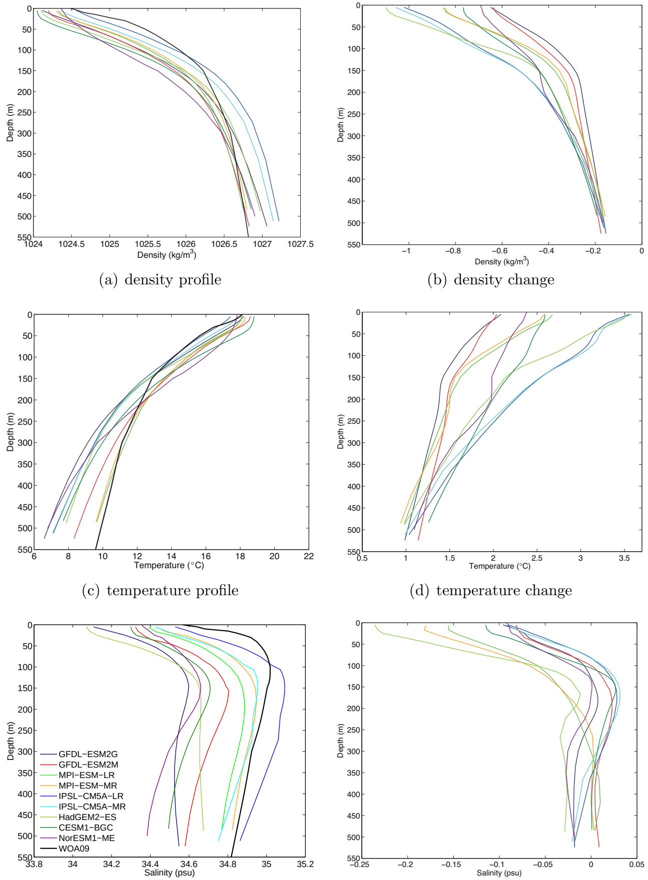

(a) density profile (b) density change

(c) temperature profile (d) temperature change

(e) salinity profile (f) salinity change

Figure 2. Mean vertical profiles are shown for density **(a)**, temperature **(c)** and salinity **(e)** for the 1990s. Changes between the 2090s–1990s are shown in **(b)**, **(d)** and **(f)**, for the same variables. Solid black line denotes WOA2009 data.

BGD

12, 12851–12897, 2015

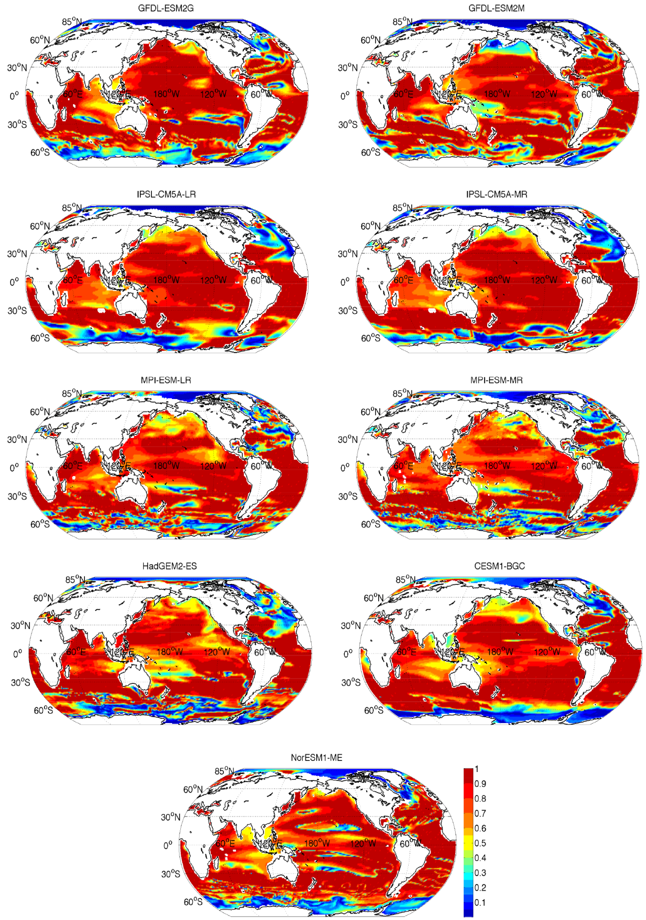

Figure 3. Fractional contribution of temperature to the stratification change from the 1990s to the 2090s is shown for each model.

BGD
12, 12851–12897, 2015

Title Page
Abstract | Introduction
Conclusions | References
Tables | Figures
◂◂ | ▸▸
◂ | ▸
Back | Close
Full Screen / Esc
Printer-friendly Version
Interactive Discussion

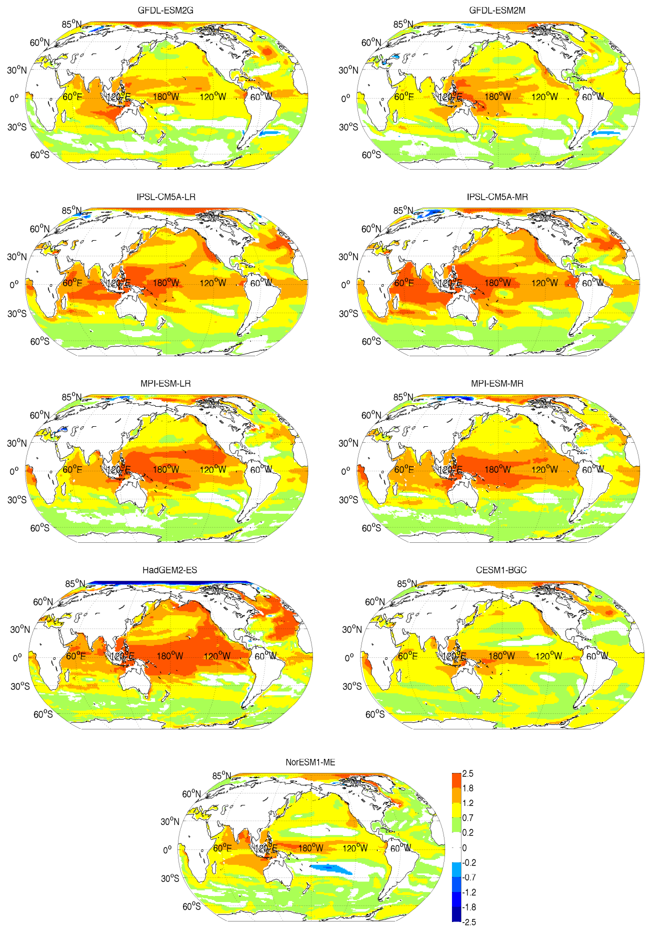

Figure 4. The spatial pattern for changes in stratification intensity changes between the 1990s and the 2090s.

BGD
12, 12851–12897, 2015

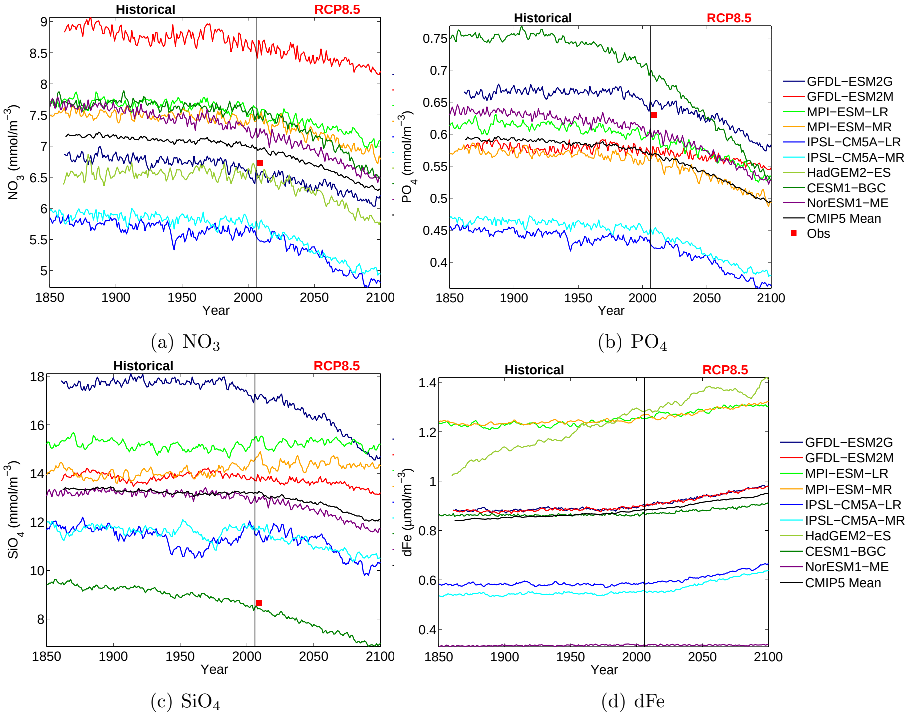

Figure 5. Time series of nitrate (NO_3), phosphate (PO_4), silicate (SiO_4) and dissolved iron (dFe) concentrations (0–100 m) are shown for 1850–2100. Red square indicates WOA2009 global mean values.

BGD
12, 12851–12897, 2015

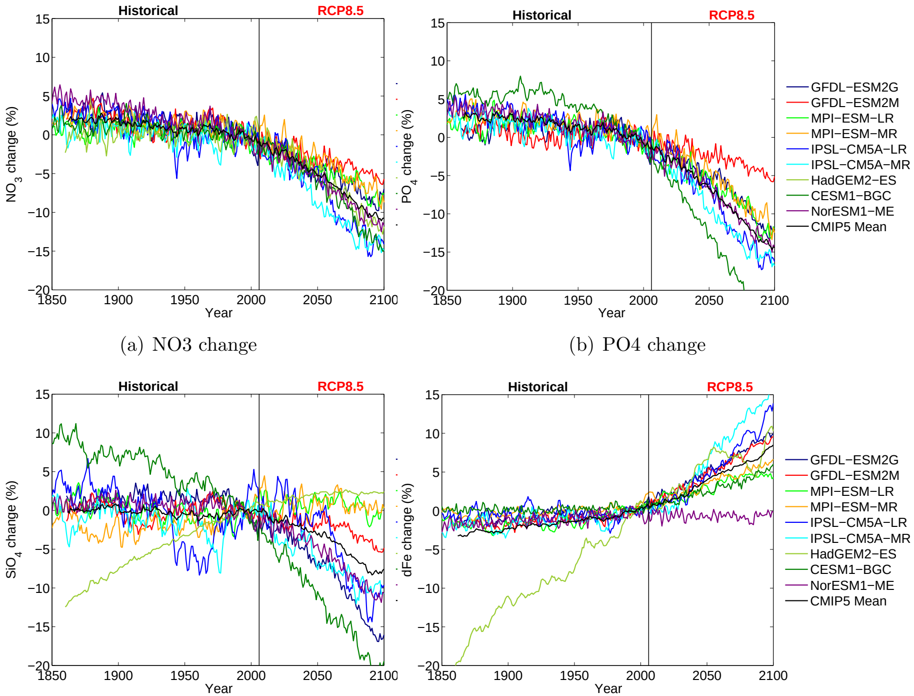

(a) NO3 change (b) PO4 change
(c) SiO4 change (d) dFe change

Figure 6. Time series are displayed of mean changes (in percent) relative to the 1990s for **(a)** NO_3, **(b)** PO_4, **(c)** SiO_4 and **(d)** dFe (0–100 m) during 1850–2100.

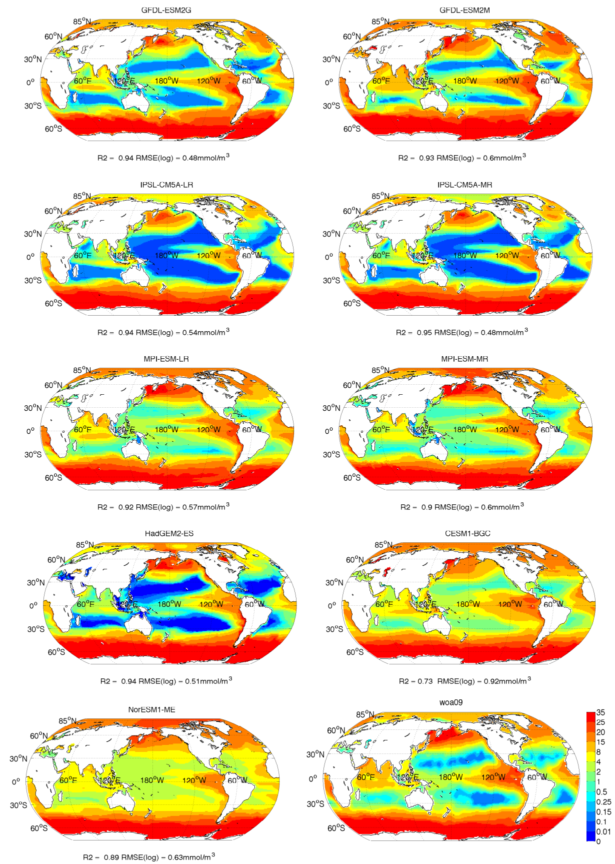

Figure 7. Mean NO_3 concentrations in the first 100 m for the1990s, *R* squared and logarithmic transformed root mean square error (RMSE) are indicated relative to observations from the WOA2009.

BGD
12, 12851–12897, 2015
Climate change impacts on net primary production (NPP)
W. Fu et al.

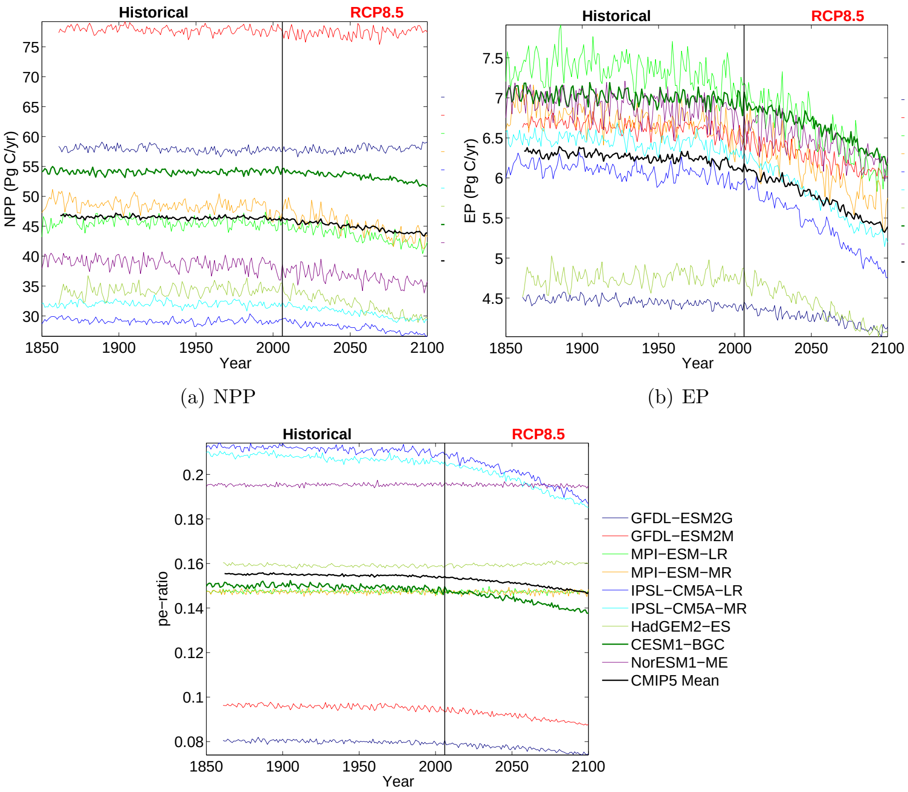

(c) pe-ratio

Figure 8. Time series of global mean net primary production, export production, and the particle export ratio over 1850–2100 are shown for each model.

BGD
12, 12851–12897, 2015

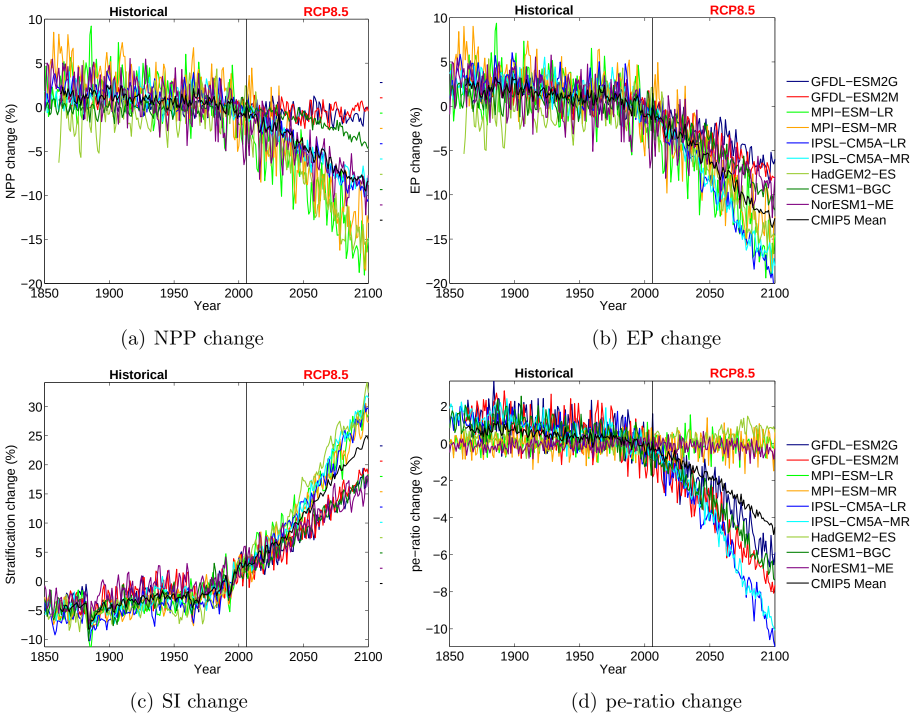

Figure 9. Time series are displayed of the percent changes in net primary production, export production, and the particle export ratio, and stratification over the period 1850–2100 (each relative to the 1990s means).

BGD
12, 12851–12897, 2015

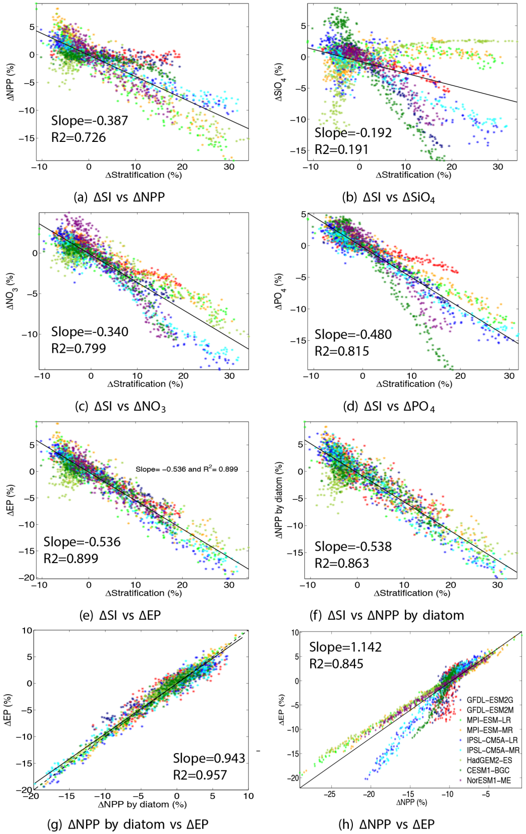

Figure 10. Relationships are shown between the relative percent change in surface stratification with climate and the relative change in several biogeochemical variables including net primary production (NPP) **(a)**, silicate **(b)**, nitrate **(c)**, phosphate **(d)**, export production (EP) **(e)**, the fraction of NPP by diatoms **(g)**. EP is plotted against the change in the fraction of NPP by diatoms **(g)** and against the change in NPP **(h)**. All changes are relative to the 1990s and plotted over 1850–2100. These time series are derived from global annual mean data.

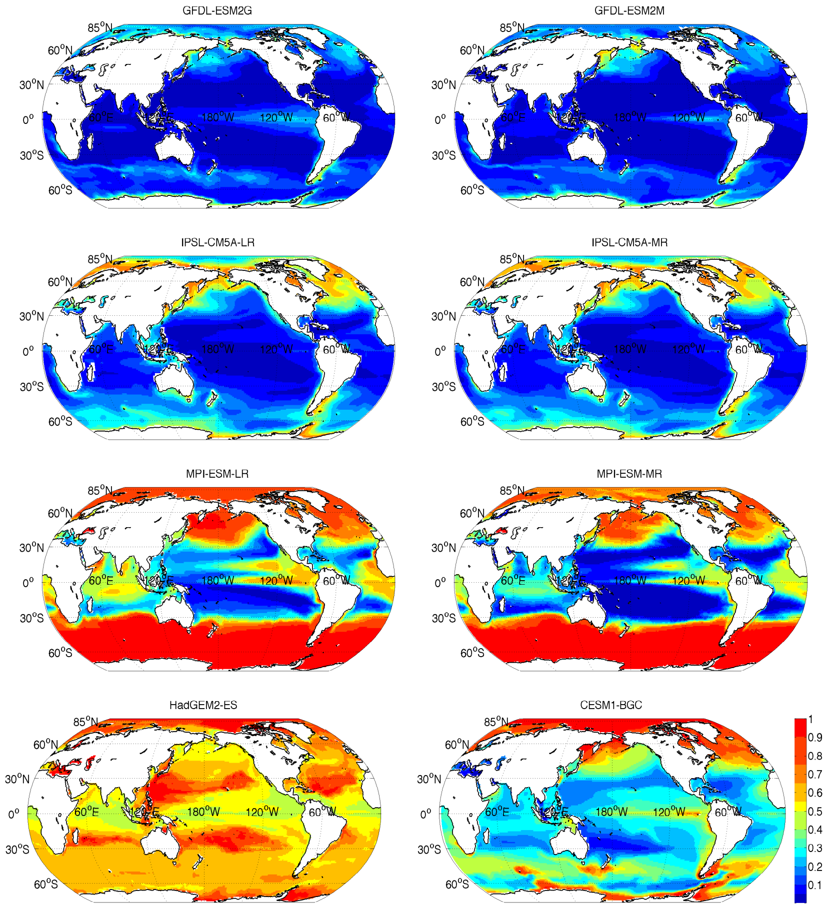

Figure 11. The fraction of total NPP by diatoms for the 1990s is shown for each model (data for NorESM not available).

BGD
12, 12851–12897, 2015
Climate change impacts on net primary production (NPP)
W. Fu et al.

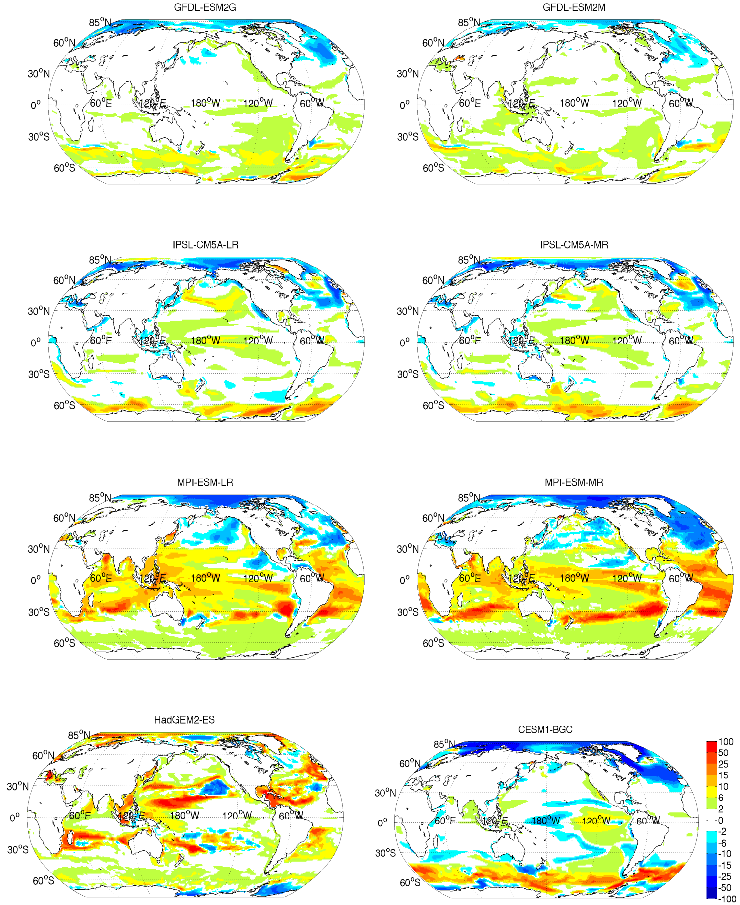

Figure 12. The percent change in NPP by diatoms between the 2090s and the 1990s.

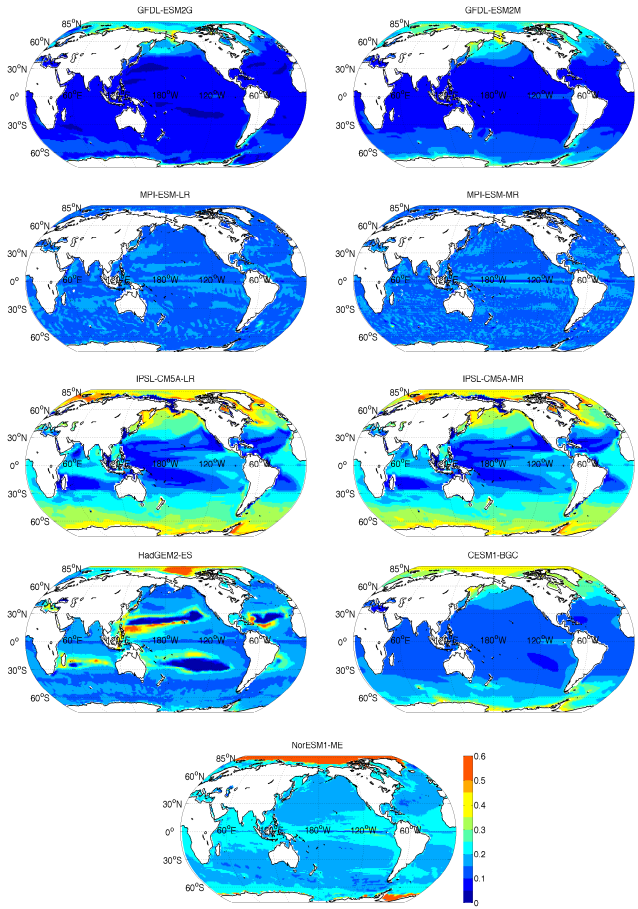

Figure 13. The mean particle export ratio for the 1990s is shown for each model.

BGD

12, 12851–12897, 2015

Climate change impacts on net primary production (NPP)

W. Fu et al.

Title Page
Abstract
Introduction
Conclusions
References
Tables
Figures
◂◂
▸▸
◂
▸
Back
Close
Full Screen / Esc
Printer-friendly Version
Interactive Discussion

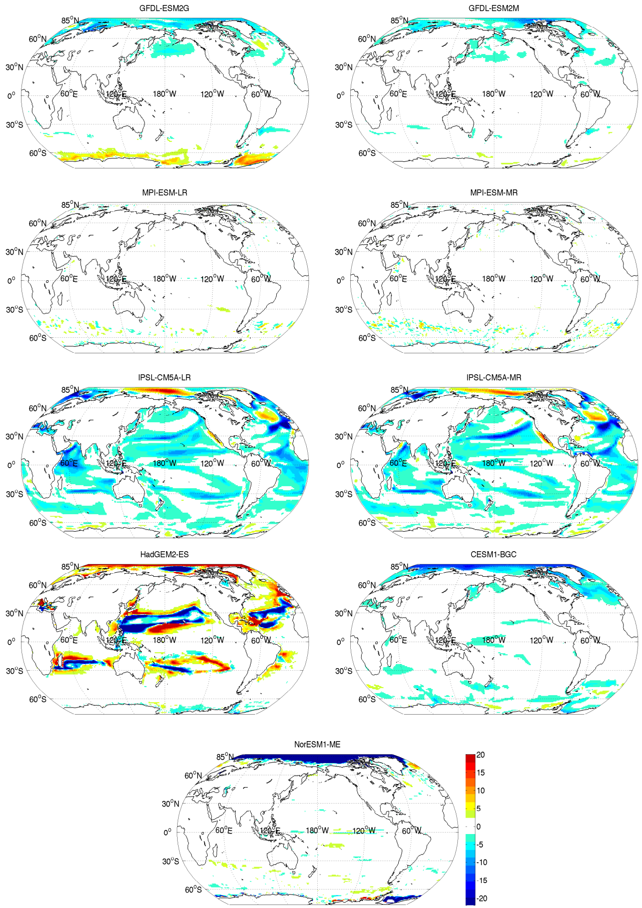

Figure 14. The percent change in particle export ratio between the 2090s and the 1990s.

BGD
12, 12851–12897, 2015

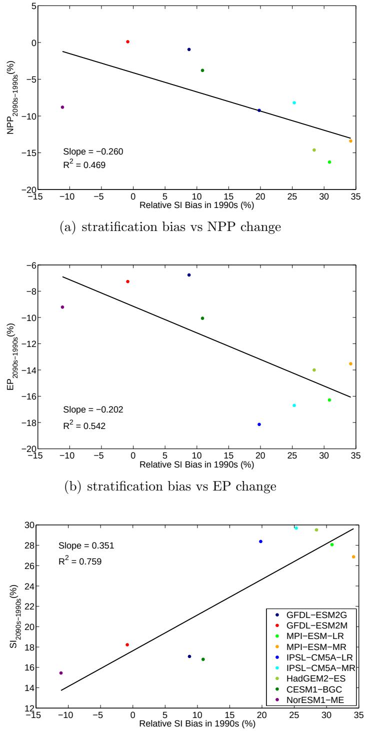

(a) stratification bias vs NPP change

(b) stratification bias vs EP change

(c) stratification bias vs stratification change

Figure 15. The stratification bias for the 1990s is plotted for each model vs. the relative changes in NPP **(a)**, EP **(b)**, and stratification **(c)** with climate change (2090s–1990s).

BGD
12, 12851–12897, 2015

Climate change impacts on net primary production (NPP)

W. Fu et al.